

International Atomic Energy Agency

INDC(PAK)-008

Distrib.: L

INDC

INTERNATIONAL NUCLEAR DATA COMMITTEE

**THE GLOBAL OPTICAL POTENTIALS AND NEUTRON - NUCLEUS
SCATTERING DATA**

I.E. Qureshi, and Q.H. Khan
Radiation Physics Division, PINSTECH, P.O. Nilore
Islamabad, Pakistan

November 1993

IAEA NUCLEAR DATA SECTION, WAGRAMERSTRASSE 5, A-1400 VIENNA

**THE GLOBAL OPTICAL POTENTIALS AND NEUTRON - NUCLEUS
SCATTERING DATA**

I.E. Qureshi, and Q.H. Khan
Radiation Physics Division, PINSTECH, P.O. Nilore
Islamabad, Pakistan

November 1993

**Reproduced by the IAEA in Austria
November 1993**

93-04975

THE GLOBAL OPTICAL POTENTIALS AND NEUTRON - NUCLEUS SCATTERING DATA

I.E. QURESHI, AND Q.H. KHAN

Radiation Physics Division, PINSTECH, P.O. Nilore
Islamabad (PAKISTAN)

We have compared the predictions of three global optical potentials with the (21.6 MeV) neutron-nucleus elastic scattering data. Nine nuclides within the mass range $40 \leq A \leq 209$ were chosen for this comparative study. By fitting the differential cross-section data with Legendre polynomials, it was possible to plot the ratio of theoretical and experimental cross sections as a function of scattering angle. Significant deviations of this ratio occur at the positions of diffraction maxima and minima. The integrated quantities i.e. total elastic cross sections, volume integrals and mean-square-radii for the three potentials under consideration have also been calculated and compared with the corresponding values obtained by using individual best fit potentials.

1. Introduction

The neutron optical model potential has been widely used for the analysis of neutron scattering and reaction data. It not only provides a convenient means of calculating total cross sections and shape elastic angular distributions but also generates distorted waves and transmission coefficients which are used in DWBA analyses and Hauser-Feshbach statistical theory for neutron induced reactions. Attempts [1,2,3] have been made to derive this potential microscopically i.e. starting from a realistic internucleon force and making use of nuclear structure information. However, most commonly it is derived in a phenomenological manner, based on assumed form factors and a number of fitted strength and geometry parameters. The phenomenological potentials may be divided into the categories of 'specific' fits and 'global' fits. The former yield parameters which pertain to a particular projectile-target combination and a specific incident energy. The latter involve parameters which are smooth functions of target A and Z and projectile energy. Such potentials can, therefore, be used to predict cross sections in those situations where experimental data is lacking, such as in astro-physical and reactor engineering applications. Many attempts have been made over the years [4,5,6,7,8,9,10] to produce global optical potentials by

using the then available experimental data on neutron and proton elastic scattering and (in some cases) polarizations. Relatively recently a new global fit has been obtained by Varner et al. [11] who have used 6000 proton and 3000 neutron data points to find 22 parameters within spherical optical model approach, using Woods-Saxon form-factors

Since neutron-nucleus global potentials have been obtained in the past with a relatively smaller data set and a rather restricted parameter space, the new fit affords the possibility of re-evaluating global potential's efficacy in reproducing aspects of specific scattering data. Some special features of the new parameterization [11] are,

1. The χ^2 is considerably reduced e.g. it is 1/3 of that obtained in ref. [7].
2. The isovector strength is 1/2 of the one used in usual analyses which means a greater reliability of the potential for applications to unstable nuclei.
3. There is an off-set term in radius parameters which is well-known in nuclear charge radii and is also expected for nuclear matter radii.
4. A smooth transition from low energy surface absorption to high energy volume absorption is generated by using smooth energy dependence (i.e. Woods-Saxon) of the strength of imaginary potential.

In spite of the difficulties associated with the use of global potentials such as the unsatisfactory extrapolation to negative energies, over-estimation of neutron total cross sections, discrepancies near Fermi energy and inherent (continuous and discrete) ambiguities, the model has rich possibilities of continuous use in nuclear data analysis for technological applications. Some of the above mentioned problems are being tackled by using dispersion relations which relate the real and imaginary parts of the potential (e.g. ref.12). Some discrepancies at low energies have been shown to be rectified by the introduction of energy dependent geometry parameters [13].

Whereas it is well-known that any global potential will not reproduce the neutron angular distributions for specific nuclides, however, it is still interesting to gauge the extent to which this is possible by better parameterization methods and strategies.

In this report we have calculated the ratios of theoretical differential cross-sections and the corresponding experimental values at different angles for 21.6 MeV neutron scattered off a number of nuclides in the mass range $40 \leq A \leq 209$. This was done by first fitting the experimental

data with sum of Legendre Polynomials. The deviation of this ratio from unity throughout the angular range is a measure of angular distribution mismatch. For the sake of comparisons, apart from Varner et al. [11] we have chosen two of the well-known and widely used parameterizations, Becchetti and Greenlees [17] and Rapaport et al. [10], and performed similar calculations with their parameters.

For the experimental data we have selected nine nuclides (Ca, Cr, Fe, Co, Ni, Y, Ce, Pb and Bi) and used neutron-nucleus differential cross section measurements of Olsson et al. [14]. These experiments were performed with 21.6 MeV mono energetic neutrons using the improved Studsvik fast neutrons time-of-flight facility. The data are highly accurate owing to the use of voltage dividers with very good timing and linearity properties and a special method of calibrating the angular position with respect to the zero point of the scattering angle. The energy resolution of 0.5 MeV was obtained and the angular uncertainties were negligible ($< 0.1^\circ$) for the purpose of theoretical analysis.

In section 2, the analytical form of the spherical optical potential is given along with the parameters of ref. 7, 10 and 11. In section 3, the method of computation is outlined and the quantities compared are described. The results are discussed in section 4.

2. Spherical Optical Model Potential

The spherical optical model potential for neutrons of energy E is most commonly represented as,

$$-U(r,E) = V(r,E) + i W(r,E) \quad (1)$$

where

$$V(r,E) = V_R(E) f_R(r) - V_{S.O.} \left(\frac{\hbar}{m_\pi c^2} \right) r^{-1} \frac{d}{dr} (f_{S.O.}(r) \underline{\sigma} \cdot \underline{1}) \quad (2)$$

$$W(r,E) = W_V(E) f_V(r) - 4a_D W_D \frac{d}{dr} (f_D(r)) \quad (3)$$

$$f_i(r) = [1 + \exp(r - R_i/a_i)]^{-1} \quad (4)$$

$$R_i = r_i A^{1/3} \quad (5)$$

In the above eqs., the potential depths V_R , $V_{S.O.}$, W_V and W_D correspond to the 'central real', 'spin-orbit', 'volume absorption' and 'derivative' terms (for surface absorption) respectively. The geometry parameters r_i and a_i appearing in the assumed Woods-Saxon form-factors $f_i(r)$ are usually

Table 1: Global optical potential parameters for 21.6 MeV neutron-nucleus scattering (1a)
Mass dependent parameters (1b) Mass independent parameters

(a)

V_R (MeV)			W_D (MeV)			r_R (fm)	$r_D=r_V$ (fm)	$r_{S.O.}$ (fm)
(1)*	(2)*	(3)*	(1)	(2)	(3)	(3)	(3)	(3)
Ca 49.388	74.71	46.42	7.6	5.576	5.218	1.18	1.2	0.972
Cr 47.542	45.631	45.42	6.677	4.776	4.593	1.186	1.21	1.007
Fe 47.674	45.734	45.491	6.743	4.833	4.638	1.187	1.213	1.016
Co 47.354	45.486	45.309	6.583	4.695	4.53	1.188	1.215	1.023
Ni 48.560	46.422	45.972	7.186	5.217	4.938	1.188	1.214	1.021
Y 46.422	44.764	44.813	6.117	4.291	4.215	1.196	1.228	1.07
Ce 45.274	43.875	44.191	5.543	3.793	3.826	1.204	1.241	1.115
Pb 44.311	43.128	43.67	5.061	3.376	3.501	1.209	1.251	1.149
Bi 44.45	43.236	43.745	5.131	3.436	3.548	1.209	1.251	1.149

(b)

W_V (MeV)	a_R (fm)	a_D, a_V (fm)	$a_{S.O.}$ (fm)	$V_{S.O.}$ (MeV)	r_R (fm)	$r_D=r_V$ (fm)	$r_{S.O.}$ (fm)
(1) 3.192	0.75	0.58	0.75	6.2	1.17	1.26	1.01
(2) 3.908	0.663	0.59	0.75	6.2	1.198	1.295	0.75
(3) 2.904	0.69	0.72	0.65	5.9	Table 1.(a)	Table 1.(a)	Table 1.(a)

- * (1) Becchetti and Greenlees. (ref 7)
- (2) Rapaport et al (ref. 10)
- (3) Varner et al (ref 11)

considered to be independent of energy and mass. However in Varner's fit the reduced radius parameters r_i depend on target mass number A.

For the nine elements chosen for this study, the potential parameters based on Varner's fit [11], Rapaport et al. fit [10] and Becchetti and Greenlees's fit [7] are given in table 1.

3. Computations and Comparisons

The computations have been performed by using the optical model code "SCAT2" [16]. The code is applicable for central spherical potentials without parameter optimization. The Schrodinger equation is solved using

Cowell's method with a number of inbuilt options of potentials for neutrons, deuterons, tritons, He-3 and alpha particles. The program calculates the shape elastic differential cross sections, compound nucleus cross sections, total cross sections, and transmission coefficients for each partial wave. In order to make a quantitative estimate of the deviation of differential cross sections produced by global potentials as compared to experimental values we have considered the Legendre polynomial fit for Olsson et al's data as reference fit. For this purpose we have fitted the experimental differential cross-sections with a sum of Legendre polynomial,

$$d\sigma/d\Omega (\theta) = \sum_{L=0}^{L_{\max}} a_L P_L (\cos\theta) \quad (6)$$

The fits have been obtained by using the same L_{\max} values as reported by Olsson et al. The resulting values pass through all the data points. The values of differential cross-sections obtained by using different global potentials relative to the Legendre fit values afford a useful basis of

comparison. Thus the ratio $(d\sigma/d\Omega)_{\text{global pot.}} / (d\sigma/d\Omega)_{\text{Legendre fit}}$ when

plotted as a function of scattering angle gives a picture of the extent to which the predictions of global potential agree with the data at different angles. These ratios for the nine elements under consideration are plotted in figs. 1-3.

The comparison of integrated quantities is also relevant due to the well-known ambiguities of optical potential parameters. Therefore we have calculated and compared the volume integrals

$$JV_R/A = \int V_R f_R(r) d^3r \quad (7)$$

$$JW_I/A = \int W(r,E) d^3r \quad (8)$$

and mean square radii

$$\langle r^2 \rangle_i = \int f_i(r) r^2 d^3r / \int f_i(r) d^3r \quad (9)$$

These are given in table 2. The computed and experimental total cross sections, are given in table 3.

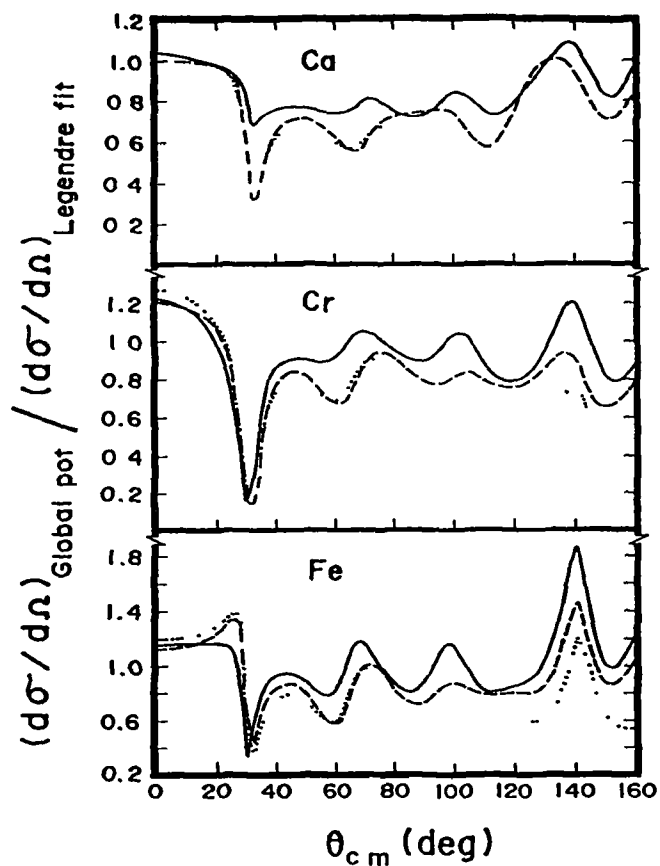


Fig 1 The differential cross-section in the case of 21.6 MeV neutron-nucleus elastic scattering is calculated using global optical potentials. The data [14] for the same reaction is fitted by a sum of Legendre polynomials. The ratio of the two cross sections are then plotted as a function of the scattering angle in the centre of mass frame for the target nuclei indicated in the diagram. The three curves in each diagram correspond to the potentials of Bechetti and Greenless [7] (), Rapaport et al [10] (-----) and Varner et al [11] (—)

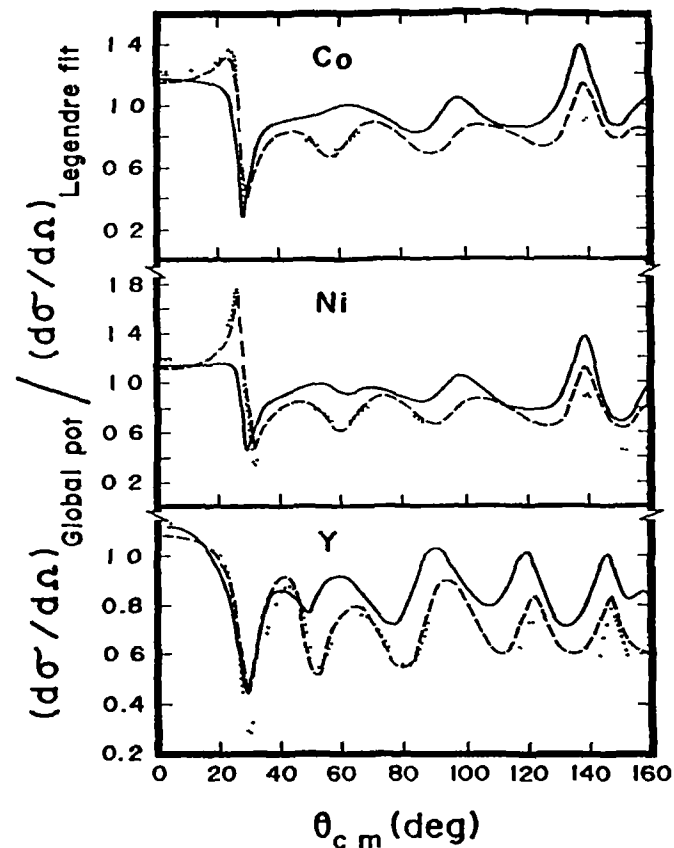


Fig 2. The differential cross-section in the case of 21.6 MeV neutron-nucleus elastic scattering is calculated using global optical potentials. The data [14] for the same reaction is fitted by a sum of Legendre polynomials. The ratio of the two cross sections are then plotted as a function of the scattering angle in the centre of mass frame for the target nuclei indicated in the diagram. The three curves in each diagram correspond to the potentials of Bechetti and Greenless [7] (), Rapaport et al [10] (-----) and Varner et al [11] (—)

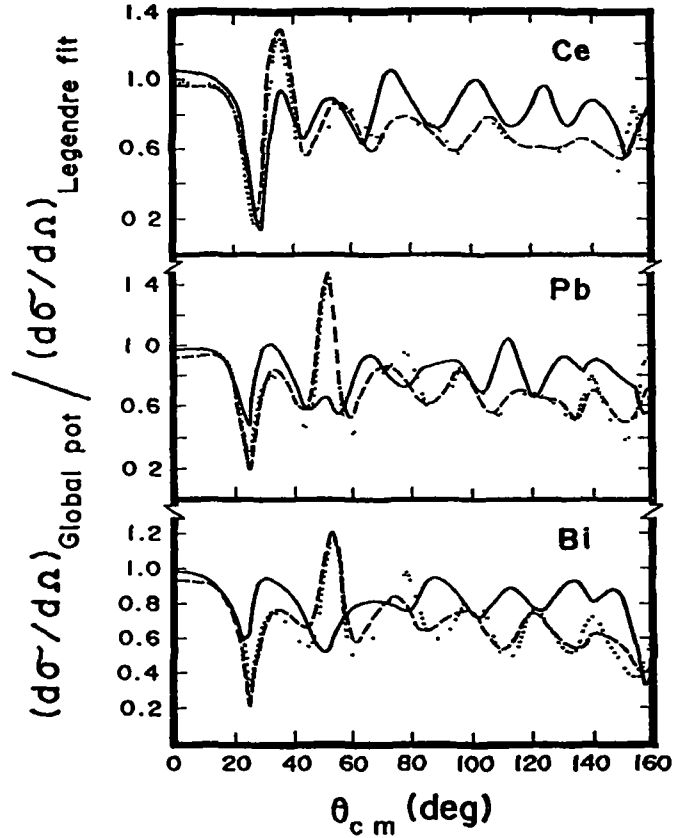


Fig 3.

The differential cross-section in the case of 21.6 MeV neutron-nucleus elastic scattering is calculated using global optical potentials. The data [14] for the same reaction is fitted by a sum of Legendre polynomials. The ratio of the two cross sections are then plotted as a function of the scattering angle in the centre of mass frame for the target nuclei indicated in the diagram. The three curves in each diagram correspond to the potentials of Becchetti and Greenless [7] (—), Rapaport et al [10] (-----) and Varner et al [11] (.....)

Table 2: The volume integrals and root-mean-square radii derived from different optical potential parameters for (21.6 MeV) neutron-nucleus elastic scattering

	JV_R/A (MeV-fm ³)				JW_I/A (MeV-fm ³)				$\langle r^2 \rangle^{1/2}$ (fm)			
	(1)*	(2)*	(3)*	(4)*	(1)	(2)	(3)	(4)	(1)	(2)	(3)	(4)
Ca	446.2	426.5	411.6	416.8	140.5	127.6	115.0	101.3	4.77	4.47	4.54	4.13
Cr	411.8	400.0	393.5	372.6	117.7	107.5	97.6	83.3	4.93	4.66	4.74	4.34
Fe	408.4	397.4	391.3	388.0	116.0	106.3	96.5	95.8	4.98	4.72	4.79	4.29
Co	402.7	392.9	388.5	391.3	112.3	103.0	93.7	91.1	5.02	4.77	4.84	4.34
Ni	414.0	401.8	394.6	392.4	120.4	110.5	100.1	96.1	5.01	4.75	4.82	4.36
Y	374.8	371.3	374.2	371.7	95.2	88.6	80.8	72.6	5.36	5.16	5.24	4.79
Ce	349.4	351.4	361.7	360.7	79.5	75.5	68.9	61.4	5.85	5.7	5.79	5.46
Pb	331.6	337.4	353.3	356.5	68.7	66.5	60.5	56.5	6.38	6.28	6.38	6.15
Bi	332.5	338.1	352.9	353.6	69.1	67.0	60.9	56.9	6.39	6.28	6.39	6.18

- * (1) Becchetti and Greenless (ref. 7)
- (2) Rapaport et al. (ref. 10)
- (3) Varner et al. (ref. 11)
- (4) Specific Fits of Olsson et al. (ref. 14)

Table 3. (a) The total cross sections σ_T for (21.6 MeV) n+nucleus interaction calculated by using global optical potential parameters and compared with the corresponding experimental values (ref 17 & 18) (b) Similar comparison for the angle integrated elastic cross-sections σ_{el} for the same reactions. The Legendre fit values pertain to the data of ref 14

(a)					(b)			
σ_T (b)					σ_{el} (b)			
	(1) [*]	(2) [*]	(3) [*]	Experimental	(1)	(2)	(3)	Legendre Fit
Ca	2.15	2.11	2.15	2.13	0.898	0.901	0.948	1.016
Cr	2.38	2.32	2.34	2.15	0.993	0.980	1.004	0.966
Fe	2.47	2.41	2.43	2.25	1.031	1.013	1.031	0.947
Co	2.53	2.48	2.49	2.32	1.061	1.043	1.06	0.987
Ni	2.54	2.48	2.50	2.35	1.058	1.035	1.047	0.982
Y	3.25	3.19	3.24	3.20	1.461	1.432	1.467	1.464
Ce	4.46	4.43	4.58	4.5	2.223	2.215	2.357	2.392
Pb	5.63	5.63	5.81	5.95	2.902	2.91	3.08	3.245
Bi	5.64	5.64	5.82	5.90	2.903	2.912	3.08	3.353

- * (1) Becchetti and Greenlees et al (ref. 7)
- (2) Rapaport et al. (ref. 10)
- (3) Varner et al (ref 11)

4. Discussion

The values of differential cross sections calculated with the help of three different global optical potentials for 21.6 MeV neutron-nucleus interaction have been divided by their corresponding Legendre fit values. These ratios are shown in figs. 1-3. Since the Legendre fits depend on the experimental data which is limited to about 160° in the c.m. frame, therefore the angular range for comparison has been chosen to be 0° - 160° . The deviation of this ratio from unity serves as a reasonably good indicator of the limitations of global potentials. The ratios as a function of angle clearly highlight the following features.

1. For the most part of the angular range, the predictions of all global potentials chosen in this study, underestimate the differential cross sections of the selected reactions. However the Varner's potential [11] yields the highest values which are, therefore, nearest to unity.
2. The fluctuations in the ratio reflect angular shifts between the 'experimental' and theoretical diffraction patterns of elastic

scattering data. Usually, the cross sections are poorly reproduced at the position of maxima and minima. The disagreement at the positions of first minima is invariably the most pronounced. There could be as much as 80% deviation at these points. For Varner's potential [11], the predicted cross sections for most nuclei remain around 20% at variance with Legendre fit values for the region beyond first diffraction minima.

3. The predicted total cross sections based on calculations with Rapaport et al. [10] potential are systematically lower compared to those of Varner et al. [11] potential. The latter are closer to experimental values only for Pb and Bi case. For other nuclides the Rapaport values are in equal or slightly better agreement with the experimental values. Similarly both of the potentials of ref. 7 and 10 yield smaller values for the total elastic cross sections compared to the predictions of ref. 11 except for Ni where the potential of ref. 7 gives higher value. The deviations of Varner's potential predictions compared to experimental total cross section vary from 1%-9% for the chosen nuclei.

In the light of the above observations, it is obvious that the global potentials should be used for application purposes with considerable caution leaving error margins sufficient to accommodate large deviations at certain angles. For the limited number of reactions investigated at a single fixed energy, it seems that Varner's potential is somewhat better than the older but widely used potentials of ref. 7 and 10.

So far as the integrated quantities viz. total elastic cross sections, volume integrals and root-mean-square radii are concerned, they are very close for all the three potentials in the region of $A=40-209$. For the integrated elastic cross sections, we may consider the values obtained by using the Legendre fit to the experimental data as "Experimental" total elastic cross sections. These values differ from those based on Varner et al. potential [11] by 0.2% (Yttrium) to 8.8% (Iron). The predictions of other two potentials are worse. The volume integrals for both real and imaginary potentials have been obtained by Olsson et al. on the basis of individual best fit optical potentials. If we consider these values as reference values then the corresponding values for the potential of Varner et al. are mostly in better agreement with the reference values except for Co and Y for which Rapaport potential yields closer values in the case of central-real part of potential. The volume integrals of imaginary potentials in the case of Varner et al. are consistently smaller than the other two

global potentials and agree more closely to the individual best fit value. However the Varner's potential based mean-square-radii (corresponding to the real potential geometry) are in greater disagreement with the individual best fit based values. Here the Rapaport potential yields the best agreement.

5. Conclusions

The inter-comparison of calculations based on three global optical potentials has been made in the case of 21.6 MeV neutron nucleus scattering. Considering a fitted Legendre polynomial as a reference fit, the predictions of three potentials for differential cross sections are found to show large deviations at the positions of diffraction minima. The potential of ref.11 (Varner et al.) produces the results closest to reference fit values for the differential cross sections. The integrated quantities in all the three cases yield fairly close values. However Varner's potential parameters yield values closer to the experimental reference values in most cases. The root-mean-square-radii for the potential of ref.11 are in relatively greater disagreement with the individual best fit values compared to the other two potentials.

REFERENCE

1. Jeukenne, J.-P., Lejeune, A., Mahaux, C.: Phys. Rev. C15, 10 (1977)
Jeukenne, J.-P., Lejeune, A., Mahaux, C.: Phys. Rev. C16, 80 (1977)
2. Brieva, F.A., Rook, J.R.: Nucl. Phys. A291, 2990 (1977)
Brieva, F.A., Rook, J.R.: Nucl. Phys. A297, 206 (1978)
Brieva, F.A., Rook, J.R.: Nucl. Phys. A307, 493 (1978)
3. Yamaguchi, N., Nagata, S., Matsuda, T.: Prog. Theor. Phys 70, 459 (1983)
4. Perey, F.G., Buck, B.: Nucl. Phys. 32, 353 (1962)
5. Wilmore, D., Hodgson, P.E.: Nucl. Phys. 55, 673 (1964)
6. Engelbrecht, C.A., Fiedeldey, H.: Ann. Phys. 42, 262 (1967)
7. Becchetti F.D., Greenlees, G.W.: Phys. Rev. 182, 1190 (1969)
8. Patterson, D.G. et al.: Nucl. Phys. A263, 261 (1976)
9. Madland D.C., Young, P.G.: Proc. of the International Conf. on Neutron Physics and Nuclear Data for Reactors and other Applications, Harwell, OECD, p. 349 (1978)

10. Rapaport J. et al.: Nucl. Phys. A330, 15 (1979)
11. Varner, R.L. et al.: Phys. Lett. B185, 6 (1987)
12. Lawson, R.D. et al.: Phys. Rev C34, 1599 (1987)
13. Konshin V.A., Konshin, O V.: Proc. of the Workshop on Applied Nuclear Theory and Nuclear Model Calculations for Nuclear Technology Applications, Trieste, Italy, p.459 (1988)
14. Olsson, N. et al.: Nucl. Phys. A472, 237 (1987)
15. Holmqvist, B. et al.: Nucl. Phys. A146, 321 (1970)
16. Bersillon, O: Proc. of the Workshop on Applied Nuclear Theory and Nuclear Model Calculations for Nuclear Technology Applications, Trieste, Italy, p. 319 (1988)
17. Garber D.I. Kinsey, R.R. BNL 325, 3rd ed. vol II (1976)
18. Poenitz, W.P., Whalen, J.F. ANL/NDM-80 (1983)